

OT-DETECTOR: Delving into Optimal Transport for Zero-shot Out-of-Distribution Detection

Yu Liu^{1,*}, Hao Tang^{2,*}, Haiqi Zhang¹, Jing Qin² and Zechao Li^{1,†}

¹School of Computer Science and Engineering, Nanjing University of Science and Technology

²Centre for Smart Health, The Hong Kong Polytechnic University

{yu.liu, zhanghq2017, zechao.li}@njust.edu.cn, {howard-hao.tang, harry.qin}@polyu.edu.hk

Abstract

Out-of-distribution (OOD) detection is crucial for ensuring the reliability and safety of machine learning models in real-world applications. While zero-shot OOD detection, which requires no training on in-distribution (ID) data, has become feasible with the emergence of vision-language models like CLIP, existing methods primarily focus on semantic matching and fail to fully capture distributional discrepancies. To address these limitations, we propose OT-DETECTOR, a novel framework that employs Optimal Transport (OT) to quantify both semantic and distributional discrepancies between test samples and ID labels. Specifically, we introduce cross-modal transport mass and transport cost as semantic-wise and distribution-wise OOD scores, respectively, enabling more robust detection of OOD samples. Additionally, we present a semantic-aware content refinement (SaCR) module, which utilizes semantic cues from ID labels to amplify the distributional discrepancy between ID and hard OOD samples. Extensive experiments on several benchmarks demonstrate that OT-DETECTOR achieves state-of-the-art performance across various OOD detection tasks, particularly in challenging hard-OOD scenarios.

1 Introduction

Machine learning models are typically trained and evaluated under a closed-set setting, where they are expected to classify data from a predefined set of known classes. However, in real-world scenarios, models are often faced with data from unknown classes, referred to as out-of-distribution (OOD) data. This situation is especially critical in high-stakes applications such as autonomous driving and medical diagnostics, where the failure to detect OOD data may lead to catastrophic outcomes. Therefore, accurately detecting OOD samples is essential for the safe and reliable deployment of machine learning models in practical settings [Yang *et al.*, 2024].

*These authors contributed equally to this work.

†Corresponding author

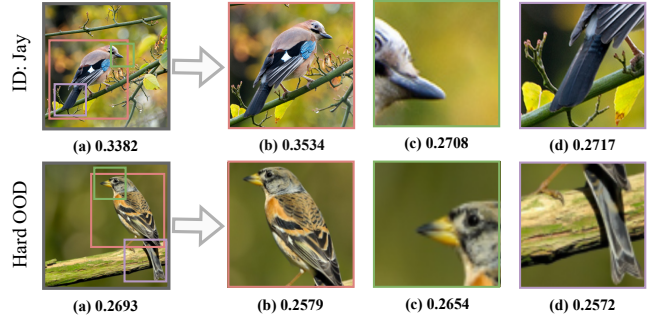


Figure 1: Illustration of diverse views containing distinct semantic information. The value beneath each view represents its cosine similarity to the text prompt “a photo of a Jay”.

Recently, the emergence of Contrastive Language-Image Pre-training (CLIP) has introduced powerful recognition and generalization capabilities [Radford *et al.*, 2021], thereby enabling various open-world recognition tasks. Building upon CLIP, several *zero-shot* OOD detection methods have been proposed. For example, ZOC [Esmailpour *et al.*, 2022] combines visual and textual embeddings to identify OOD samples, and MCM [Ming *et al.*, 2022a] employs a scaled softmax function to match test images against in-distribution (ID) labels. Beyond these approaches, some methods incorporate external knowledge. CLIPN [Wang *et al.*, 2023] pretrains an additional text encoder with a “no” logit to sharpen CLIP’s OOD sensitivity, while NegLabel [Jiang *et al.*, 2024] leverages WordNet to mine negative labels that are semantically dissimilar to ID data. However, these negative labels may not effectively capture OOD samples sharing semantic overlap with ID classes. EOE [Cao *et al.*, 2024] leverages large language models (LLMs) to generate potential OOD labels, but depending on LLMs can introduce privacy and computational concerns. Despite these advances, existing methods predominantly focus on *semantic matching* between test images and ID labels, inherently overlooking *distributional discrepancies* between ID and OOD samples. Moreover, the challenge of distinguishing hard OOD samples that are semantically similar to ID data remains largely unresolved. These gaps raise an important question:

Can we simultaneously capture both semantic and distributional cues in a zero-shot OOD detection framework, without resorting to external knowledge?

To address this issue, we first draw upon the theory of Optimal Transport (OT), a mathematical framework commonly used to quantify discrepancies between probability distributions [Courty *et al.*, 2017; Arjovsky *et al.*, 2017]. OT has shown promise in settings where known and unlabeled samples coexist [Ren *et al.*, 2024; Lu *et al.*, 2023], yet its application to *zero-shot* OOD detection is non-trivial, particularly due to the lack of ID image samples at inference. Fortunately, CLIP’s vision-text alignment can mitigate this limitation: CLIP embeds relevant text-image pairs closely together in feature space. Motivated by this property, we propose using ID text labels as proxies for ID images. By measuring cosine distances between test images and textual ID labels, OT can naturally identify the closest label for each image. Concretely, we introduce the *transport mass* in OT to represent a **semantic-wise** score, and a **distribution-wise** score to measure the *transport cost* bridging the modality gap. By strategically combining these two components, we obtain an OT-based OOD score function that captures both semantic- and distribution-level discrepancies.

However, hard OOD samples that are semantically close to ID classes can still fool CLIP by sharing common backgrounds or object attributes. As illustrated in Figure 1(b), removing ambiguous regions and emphasizing discriminative parts can improve the separability between ID and such OOD samples. Conversely, shared regions (e.g., beaks, tails) lead to low similarity scores unless more fine-grained features are highlighted. To this end, we propose a plug-and-play *Semantic-aware Content Refinement* (SaCR) module. For ID images, SaCR refines the visual content by retaining discriminative regions and better aligning features with their corresponding textual labels; for OOD samples, since OOD labels are unavailable, we use ID labels as a guide to select common regions. Consequently, shared regions remain less informative, inducing a feature shift that magnifies the distributional discrepancy between ID and hard OOD in the refined feature space.

By integrating SaCR with the proposed OT-based OOD score function, we develop a new zero-shot OOD detection framework named OT-DETECTOR. Experimental results on multiple benchmarks demonstrate that OT-DETECTOR achieves robust and reliable performance. In particular, on the ImageNet-1K OOD detection benchmark [Huang *et al.*, 2021], OT-DETECTOR attains a FPR95 of 23.65% and AUROC of 94.49%, surpassing existing methods that rely on external knowledge. Notably, OT-DETECTOR excels in hard OOD scenarios, setting new state-of-the-art results. Our main contributions are summarized as follows:

- We introduce OT-DETECTOR, a novel zero-shot OOD detection framework that exploits implicit distributional discrepancies via Optimal Transport. To the best of our knowledge, this is the first work applying OT in the zero-shot OOD detection setting.
- We propose an OT-based OOD score function that captures both semantic-level and distribution-level discrepan-

cies, as well as a parameter-free Semantic-aware Content Refinement module to further separate ID from hard OOD samples.

- Comprehensive experiments on large-scale and hard OOD benchmarks demonstrate the effectiveness of our approach, establishing new state-of-the-art performance in zero-shot OOD detection.

2 Preliminaries

2.1 Contrastive Language-Image Pre-training

CLIP [Radford *et al.*, 2021] is a multimodal model that leverages a contrastive loss to align textual and visual representations, demonstrating exceptional generalization capabilities. The model consists of a text encoder $\mathcal{T} : u \mapsto \mathbb{R}^d$ and an image encoder $\mathcal{I} : x \mapsto \mathbb{R}^d$, where u is a text sequence and x is an image. In zero-shot classification tasks, given an input image x and a set of class labels $\mathcal{Y} = \{y_i\}_{i=1}^K$, each label is first embedded into a prompt template (e.g., “a photo of a [CLASS]”), producing a textual input for the text encoder. Formally:

$$f_i^{\text{img}} = \mathcal{I}(x), \quad f_i^{\text{text}} = \mathcal{T}(\text{prompt}(y_i)), \quad (1)$$

where $\text{prompt}(\cdot)$ is an operation that inserts the class label into a predefined textual template. Finally, the predicted label \hat{y} for the image is determined by selecting the class label whose corresponding text feature has the highest cosine similarity with the image feature:

$$\hat{y} = \arg \max_{y_i \in \mathcal{Y}} \cos(f_i^{\text{img}}, f_i^{\text{text}}). \quad (2)$$

This zero-shot inference mechanism allows CLIP to generalize to novel classes not seen during training, relying solely on natural language descriptions.

2.2 Zero-shot OOD Detection with CLIP

Zero-shot OOD detection aims to distinguish out-of-distribution (OOD) samples from in-distribution (ID) samples without requiring access to labeled ID training data, leveraging the powerful generalization capabilities of CLIP. The objective is to construct a binary classifier:

$$G(x; \mathcal{Y}_{\text{id}}, \mathcal{I}, \mathcal{T}) = \begin{cases} \text{ID}, & S(x) \geq \lambda, \\ \text{OOD}, & S(x) < \lambda, \end{cases} \quad (3)$$

where x is an input image sampled from the input space $\mathcal{X} = \mathcal{X}_{\text{id}} \cup \mathcal{X}_{\text{ood}}$, with \mathcal{X}_{id} and \mathcal{X}_{ood} denoting sets of ID and OOD samples, respectively. The set \mathcal{Y}_{id} denotes the ID class labels, and λ is a threshold that determines whether a sample is classified as ID or OOD. The OOD score function S , as proposed in existing works [Ming *et al.*, 2022a; Wang *et al.*, 2023], is computed based on the cosine similarity between visual and textual features derived from Eq. (1).

2.3 Optimal Transport

Optimal Transport (OT) focuses on finding the minimum transportation distance required to transfer one distribution to another, such as the Wasserstein distance. This makes it a powerful tool for solving distribution matching problems

across various tasks. Here, we introduce OT for discrete empirical distributions.

Consider two sets, \mathcal{X} with supply samples $\{x_i\}_{i=1}^n$ and \mathcal{Y} with demand samples $\{y_j\}_{j=1}^m$, represented by the empirical distributions:

$$\mu = \sum_{i=1}^n p_i \delta_{x_i}, \quad \nu = \sum_{j=1}^m q_j \delta_{y_j}, \quad (4)$$

where δ_{x_i} is the Dirac delta measure centered at x_i . The terms p_i and q_j represent the probability masses associated with the samples, satisfying $\sum_{i=1}^n p_i = 1$ and $\sum_{j=1}^m q_j = 1$. The minimum transport distance can be determined as follows:

$$\min_{P \in U(\mu, \nu)} \langle C, P \rangle_F, \quad (5)$$

where

$$U(\mu, \nu) = \{P \in \mathbb{R}_+^{n \times m} \mid P \mathbf{1}_m = \mu, P^\top \mathbf{1}_n = \nu\} \quad (6)$$

denotes the transportation polytope of μ and ν . Here, $\mathbf{1}_n$ and $\mathbf{1}_m$ are all-one vectors of appropriate dimensions. The cost matrix $C \in \mathbb{R}^{n \times m}$ defines the transport cost between supply and demand samples, where each entry corresponds to a chosen metric such as Euclidean or Mahalanobis distance.

To enhance numerical stability and optimization convergence, Cuturi [Cuturi, 2013] introduced an entropic regularization term $H(P)$, reformulating the objective as:

$$\min_{P \in U(\mu, \nu)} \langle C, P \rangle_F - \frac{1}{\epsilon} H(P), \quad (7)$$

where $\epsilon > 0$ is the regularization hyperparameter, and

$$H(P) = - \sum_{i,j} P_{ij} \log P_{ij}. \quad (8)$$

The resulting assignment matrix can be expressed as:

$$P^\epsilon = \text{Diag}(\mathbf{a}) \exp(-\epsilon C) \text{Diag}(\mathbf{b}), \quad (9)$$

where \mathbf{a} and \mathbf{b} are non-negative vectors defined up to a multiplicative factor and can be efficiently computed using Sinkhorn’s algorithm [Cuturi, 2013]. The OT methodology used in our work is based on the above approach and will be further detailed in the following section.

3 Method

In this paper, we introduce Optimal Transport (OT) to improve the performance of zero-shot OOD detection. However, two key challenges need to be addressed:

1. **Identifying hard OOD samples** that exhibit high semantic and distributional similarity to ID samples, making them particularly difficult to detect;
2. **Quantify distributional discrepancies** between ID and OOD samples and transform them into effective OOD detection scores.

To tackle the first challenge, we propose a *Semantic-aware Content Refinement* (SaCR) module, which consists of three steps to adaptively refine both hard OOD and ID samples, as illustrated in Figure 2. By enhancing the distinguishability

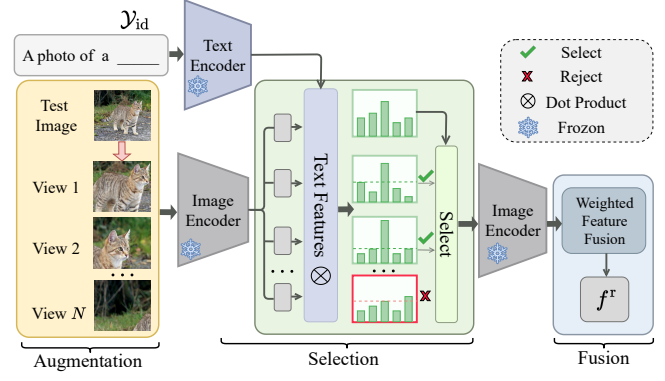


Figure 2: Pipeline of the Semantic-aware Content Refinement (SaCR) module.

Algorithm 1: Semantic-aware Content Refinement

Input : Input image x , ID labels \mathcal{Y}_{id} , Image encoder \mathcal{I} , Text encoder \mathcal{T} , Confidence function M , Top- k selection parameter k , Number of views N

Output: Refined feature f^r

- 1 $X^v \leftarrow \text{RandomCrop}(x, N)$ // Generate N views
 - 2 **for** $y_i \in \mathcal{Y}_{\text{id}}$ **do**
 - 3 $f_i^{\text{text}} \leftarrow \mathcal{T}(\text{prompt}(y_i))$ // Encode label y_i
 - 4 $\hat{y} \leftarrow \arg \max_{y_i \in \mathcal{Y}_{\text{id}}} \cos(\mathcal{I}(x), f_i^{\text{text}})$ // Predict label \hat{y}
 - 5 $X^f \leftarrow \emptyset, M^f \leftarrow \emptyset$
 - 6 **for** $x_i^v \in X^v$ **do**
 - 7 $f_i^{\text{img}} \leftarrow \mathcal{I}(x_i^v)$ // Encode view x_i^v
 - 8 $\hat{y}_i^v \leftarrow \arg \max_{y_j \in \mathcal{Y}_{\text{id}}} \cos(f_i^{\text{img}}, f_j^{\text{text}})$ // Assign label to view x_i^v
 - 9 **if** $\hat{y}_i^v = \hat{y}$ **then**
 - 10 $X^f \leftarrow X^f \cup \{x_i^v\}$
 - 11 $M^f \leftarrow M^f \cup \{M(x_i^v)\}$
 - 12 $\text{inds} \leftarrow \text{Top-K}(M^f, k)$ // Select top- k views with highest confidence
 - 13 $f^r \leftarrow \sum_{i \in \text{inds}} M(x_i^v) \cdot \mathcal{I}(x_i^v)$
-

of refined features, SaCR aims to amplify the distributional discrepancies between ID and OOD samples.

For the second challenge, we leverage OT to convert the semantic and distributional relationships between test samples and ID label space into an OOD detection score. Specifically, we incorporate two complementary components: a *Semantic-wise OOD Score* and a *Distribution-wise OOD Score*. As shown in Figure 3, we combine these two scores to develop a novel OOD detection framework, termed OT-DETECTOR, enabling reliable zero-shot OOD detection without requiring additional ID data or outlier class labels.

3.1 Semantic-aware Content Refinement

Motivation. Hard OOD samples typically exhibit similar background or object attributes to their corresponding ID

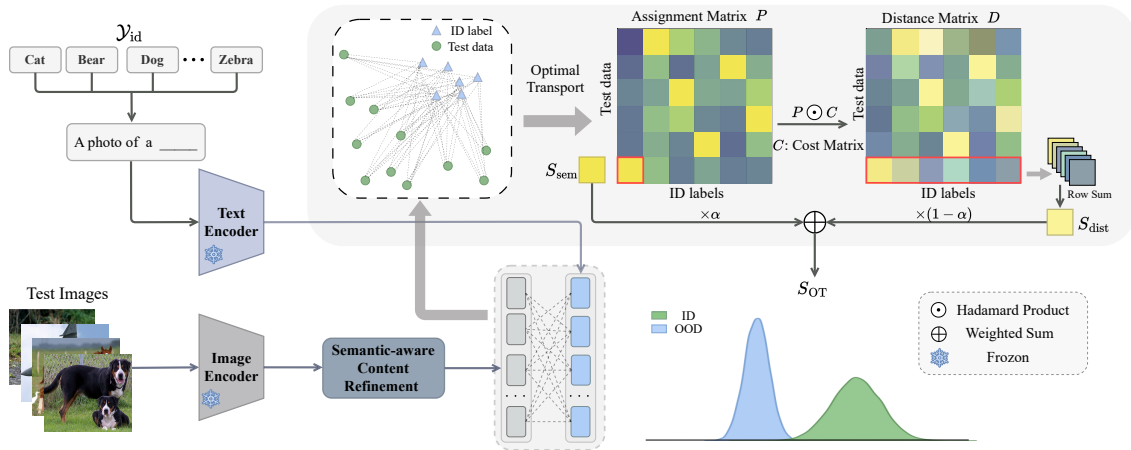


Figure 3: Pipeline of our Optimal Transport-based framework OT-DETECTOR for zero-shot OOD detection.

samples, which confuse CLIP and result in high OOD scores for these hard OOD samples. To mitigate this, we propose a *Semantic-aware Content Refinement* (SaCR) module, which adaptively refines the visual content of both ID and hard OOD samples guided by the ID label semantics, producing more discriminative visual features. By amplifying the distributional discrepancy between ID and hard OOD samples, SaCR makes it easier for the subsequent OT-based score functions to identify hard OOD samples.

View Augmentation. We start by generating multiple views of an input image to capture diverse visual information. Specifically, given a test image x and the ID label space \mathcal{Y}_{id} , we apply random cropping at various scales to yield a set of candidate views, $X^v = \{x_i^v\}_{i=1}^N$. This multi-view strategy aims to explore different local regions of x and provide a broader range of features.

View Selection. Not all views are equally relevant; some may primarily contain background or only partial object regions. We therefore discard views with predictions inconsistent with that of the original image x . Since ground-truth labels are unavailable under the zero-shot setting, we use the semantic concept of x as weak supervision. Let \hat{y} be the predicted label for x , and $\hat{Y}^v = \{\hat{y}_i^v\}_{i=1}^N$ be the predicted labels for X^v . Both \hat{y} and \hat{Y}^v are obtained via Eqs. (1) and (2) with \mathcal{Y}_{id} . We retain only the views whose predicted labels match \hat{y} , forming a refined set:

$$X^f = \{x_i^v \in X^v \mid \hat{y}_i^v = \hat{y}\}. \quad (10)$$

Next, to further select the most confident views, we define a margin function $M(\cdot)$ based on the cosine similarity logits from CLIP. For an image x , let $\text{logits}(x)$ be the sorted similarity scores (logits) over the ID labels. Then the margin $M(x)$ is the difference between the largest and the second-largest logit, i.e., $M(x) = \max \text{logits}(x) - 2^{\text{nd}} \max \text{logits}(x)$. We compute $M(x_i^f)$ for each view $x_i^f \in X^f$, rank them in descending order, and choose the top- k :

$$X^{f'} = \left\{ x_j^f \in X^f \mid j \in \text{Top-}k(\{M(x_i^f)\}_{i=1}^{N'}) \right\}. \quad (11)$$

Here, $\text{Top-}k(\cdot)$ returns the indices of the k highest margin values, and $N' \leq N$ is the number of remaining views after the label-consistency filter.

View Fusion. Finally, we fuse the selected views into a single, refined feature. Each view is first encoded by the CLIP image encoder $\mathcal{I}(\cdot)$, then weighted by its margin score and summed:

$$f^r = \text{norm} \left(\sum_{j=1}^k M(x_j^f) \cdot \mathcal{I}(x_j^f) \right), \quad (12)$$

where $\text{norm}(\cdot)$ denotes L2 normalization along the feature dimension. A step-by-step summary of this procedure is outlined in Algorithm 1.

3.2 A New OOD Detection Score

Motivation. Empirically, OOD and ID data often occupy distinct regions in the embedding space. This observation motivates us to leverage Optimal Transport (OT) to quantify this distributional discrepancy and design an effective OOD score. Since direct interaction between ID and OOD samples is not feasible, we employ ID label features as a bridge and use OT to measure the distributional difference between test samples and these label features. Specifically, we propose two complementary OT-based scores in our OT-DETECTOR, which consider both sample-level and distribution-level discrepancies:

- **Semantic-wise OOD Score:** OT assigns larger transport mass to supply samples that are closer to demand samples. Hence, the mass transported from a test sample to an ID label can reflect their semantic similarity. For OOD samples that tend to be far from all ID labels, this transported mass will be relatively small.
- **Distribution-wise OOD Score:** Considering the modality gap between textual and visual features, we further identify OOD samples by assessing the cost required for a test sample to “bridge” this gap to the ID label feature space. This cost, derived from the OT distance, indicates the distributional discrepancy.

Method	OOD Dataset									
	iNaturalist		SUN		Places		Texture		Average	
	FPR95↓	AUROC↑	FPR95↓	AUROC↑	FPR95↓	AUROC↑	FPR95↓	AUROC↑	FPR95↓	AUROC↑
MSP [Hendrycks and Gimpel, 2017]	40.89	88.63	65.81	81.24	67.90	80.14	64.96	78.16	59.89	82.04
Energy [Liu <i>et al.</i> , 2020]	21.59	95.99	34.28	93.15	36.64	91.82	51.18	88.09	35.92	92.26
Fort <i>et al.</i> [Fort <i>et al.</i> , 2021]	15.07	96.64	54.12	86.37	57.99	85.24	53.32	84.77	45.12	88.25
CLIPN [Wang <i>et al.</i> , 2023]	19.13	96.20	25.69	94.18	32.14	92.26	44.60	88.93	30.39	92.89
MCM [Ming <i>et al.</i> , 2022a]	30.91	94.61	37.59	92.57	44.69	89.77	57.77	86.11	42.74	90.77
GL-MCM [Miyai <i>et al.</i> , 2023]	15.18	96.71	30.42	93.09	38.85	89.90	57.93	83.63	35.47	90.83
EOE [Cao <i>et al.</i> , 2024]	12.29	97.52	20.40	95.73	30.16	92.95	57.53	85.64	30.09	92.96
NegLabel [Jiang <i>et al.</i> , 2024]	1.91	99.49	20.53	95.49	35.59	91.64	43.56	90.22	25.40	94.21
OT-DETECTOR (Ours)	7.91	98.16	16.18	96.15	27.43	93.30	43.07	90.34	23.65	94.49

Table 1: Performance comparison for ImageNet-1K benchmark as ID dataset with various OOD datasets.

OT Formulation. Let the test set be $\mathcal{X} = \{x_i\}_{i=1}^{|\mathcal{X}|}$ and the refined visual features (from the Semantic-aware Content Refinement module in Section 3.1) be $F^r = \{f_i^r\}_{i=1}^{|\mathcal{X}|} \in \mathbb{R}^{|\mathcal{X}| \times d}$, where $|\mathcal{X}|$ denotes the number of test samples, and d is the feature dimension. Meanwhile, we denote the CLIP textual features for all ID labels by $F^{\text{text}} = \{f_j^{\text{text}}\}_{j=1}^K \in \mathbb{R}^{K \times d}$, where K is the number of ID class labels. We assume unknown priors and define the discrete measures:

$$\mu = \sum_{i=1}^{|\mathcal{X}|} p_i \delta_{f_i^r}, \quad \nu = \sum_{j=1}^K q_j \delta_{f_j^{\text{text}}}, \quad (13)$$

with $p_i = \frac{1}{|\mathcal{X}|}$ and $q_j = \frac{1}{K}$. To construct the cost matrix $C \in \mathbb{R}^{|\mathcal{X}| \times K}$, we adopt the cosine distance since CLIP is pretrained with a contrastive objective that aligns visual and textual representations, i.e., $C = 1 - F^r (F^{\text{text}})^\top$. We then solve the following entropic regularized OT problem:

$$\min_{P \in U(\mu, \nu)} \left\langle 1 - F^r (F^{\text{text}})^\top, P \right\rangle_F - \frac{1}{\epsilon} H(P), \quad (14)$$

where $H(P)$ is the entropic regularization term, $\epsilon > 0$ is the regularization parameter, and $P^* \in \mathbb{R}^{|\mathcal{X}| \times K}$ denotes the optimal transport plan.

Semantic-wise OOD Score. The assignment matrix P^* maps $|\mathcal{X}|$ test samples to K ID labels, capturing the transport mass from each test sample x_i to every ID label. We quantify the semantic alignment by focusing on the largest transport mass for each sample. Formally, the semantic-wise score is

$$S_{\text{sem}}(x_i) = \max_j p_{ij}^*. \quad (15)$$

Intuitively, higher mass indicates stronger alignment with at least one ID label.

Distribution-wise OOD Score. The Wasserstein distance, $\sum_{i,j} p_{ij}^* c_{ij}$, reflects the overall distributional discrepancy between test samples and ID labels. We decompose it to isolate the portion that corresponds to each test sample x_i , defining the distribution-wise score as

$$S_{\text{dist}}(x_i) = 1 - \sum_{j=1}^K p_{ij}^* c_{ij}. \quad (16)$$

Here, c_{ij} is the entry of the cost matrix C , and for OOD samples, bridging the gap to the ID label space typically incurs a larger cost, leading to a lower S_{dist} .

Final OT-based OOD Score Function. We combine these two score functions in our OT-DETECTOR to effectively capture both semantic alignment and distributional discrepancy:

$$S_{\text{OT}}(x_i) = \alpha S_{\text{sem}}(x_i) + (1 - \alpha) S_{\text{dist}}(x_i), \quad (17)$$

where $\alpha \in [0, 1]$ balances the contributions of S_{sem} and S_{dist} .

4 Experiments

4.1 Experiments Setup

Datasets. Following the previous work [Ming *et al.*, 2022a], we evaluate our method on the ImageNet-1K OOD benchmark to ensure comparability with other methods. The ImageNet-1K OOD benchmark uses ImageNet-1K as the ID data and considers Texture [Cimpoi *et al.*, 2014], iNaturalist [Horn *et al.*, 2018], SUN [Xiao *et al.*, 2010], and Places365 [Zhou *et al.*, 2018] as OOD data. Additionally, we perform hard OOD analysis using semantically similar subsets of ImageNet constructed by MCM, e., ImageNet-10, ImageNet-20, and ImageNet-100, which show high semantic similarity.

Evaluation Metrics. We evaluate our method using two standard metrics: (1) **FPR95**: the false positive rate of OOD samples when the true positive rate of ID samples is at 95%; (2) **AUROC**: the area under the receiver operating characteristic curve.

Implementation Details. We utilize CLIP as the pretrained model, widely adopted in previous works. Specifically, we employ CLIP-B/16, comprising a ViT-B/16 image encoder and a masked self-attention Transformer text encoder, with weights from OpenAI’s open-source models. For view augmentation, $N = 256$ randomly cropped images are generated, and the Top- $k = 20$ crop features are selected for fusion. In the OT component, we fix $\epsilon = 90$ for entropic regularization and dynamically determine the optimal α for each OOD dataset. We also analyze the impact of different batch sizes (see Appendix A.7). Since this work does not focus on textual modality, we use a standard prompt, ”a photo of a [CLASS],” for all experiments. Further analysis on the influence of different prompts is provided in Appendix A.2.

Compared Methods. We compare our method with state-of-the-art OOD detection methods, including zero-shot methods and those requiring fine-tuning or auxiliary OOD labels. For a fair comparison, all methods are implemented

Method	ID OOD	ImageNet-10 ImageNet-20		ImageNet-20 ImageNet-10		ImageNet-10 ImageNet-100		ImageNet-100 ImageNet-10		Average	
		FPR95↓	AUROC↑	FPR95↓	AUROC↑	FPR95↓	AUROC↑	FPR95↓	AUROC↑	FPR95↓	AUROC↑
Energy [Liu <i>et al.</i> , 2020]		10.20	97.94	18.88	97.15	5.65	98.90	63.51	87.66	24.56	95.41
MCM [Ming <i>et al.</i> , 2022a]		5.00	98.71	16.99	97.69	2.29	99.31	66.37	86.45	22.66	95.54
EOE [Cao <i>et al.</i> , 2024]		4.20	99.09	15.85	97.74	5.13	98.85	68.71	85.62	23.47	95.33
NegLabel [Jiang <i>et al.</i> , 2024]		5.10	98.86	4.60	98.81	1.68	99.51	40.20	90.19	12.90	96.84
OT-DETECTOR (Ours)		2.50	99.17	3.78	99.14	3.06	99.17	22.60	96.15	7.98	98.41

Table 2: Performance comparison on hard OOD detection tasks.

using CLIP-B/16 as their backbone, consistent with our OT-DETECTOR. For methods requiring pre-training or fine-tuning, we consider MSP [Hendrycks and Gimpel, 2017], Energy [Liu *et al.*, 2020], CLIPN [Wang *et al.*, 2023], and the method proposed in [Fort *et al.*, 2021]. Among zero-shot methods, we compare against MCM [Ming *et al.*, 2022a] and GL-MCM [Miyai *et al.*, 2023]. Additionally, we evaluate our OT-DETECTOR against recently proposed representative methods, including EOE [Cao *et al.*, 2024] and NegLabel [Jiang *et al.*, 2024]. Notably, CLIPN relies on a large-scale auxiliary dataset, NegLabel leverages a large corpus database, and EOE depends on large language models. In contrast, our OT-DETECTOR operates without requiring any auxiliary datasets or candidate OOD labels.

4.2 Main Results

Evaluation on ImageNet-1K Benchmark. Table 1 shows the performance of our method on the large-scale ImageNet-1K dataset as ID data, evaluated against four OOD datasets: iNaturalist, SUN, Places, and Texture. Our method achieves state-of-the-art (SOTA) performance, with an average FPR95 of 23.65% and AUROC of 94.49%. Notably, it significantly outperforms recently proposed EOE and NegLabel. Further discussion and analysis are provided in Appendix A.8.

Evaluation on Hard OOD Detection Tasks. Table 2 presents the experimental result of our method on hard OOD detection tasks. OT-DETECTOR consistently demonstrates superior results across all four tasks. Specifically, when ImageNet-100 is used as ID data and ImageNet-10 as OOD data, our method achieves 43.78% improvement in FPR95 and 6.61% improvement in AUROC compared to NegLabel, without requiring access to potential outlier OOD labels. Finally, our method achieves an average FPR95 of 7.98% and AUROC of 98.41% on hard OOD tasks. These results highlight the outstanding effectiveness of OT-DETECTOR in tackling challenging OOD detection scenarios.

4.3 Ablation Study

Table 3 analyzes the key components of OT-DETECTOR. Initially, MCM [Ming *et al.*, 2022a] serves as our baseline when no additional modules are applied.

OT-based Score Functions. Comparing the first and second rows of Table 3, we observe that using only the semantic-wise score S_{sem} notably outperforms the baseline, indicating that the transport mass from the assignment matrix effectively captures semantic discrepancy crucial for identifying OOD samples. In contrast, comparing the first and third rows shows that the distribution-wise score S_{dist} alone achieves an FPR95

SaCR	Score Functions		FPR95↓	AUROC↑
	S_{sem}	S_{dist}		
✗	✗	✗	42.74	90.77
✗	✓	✗	31.30	92.07
✗	✗	✓	43.76	90.94
✗	✓	✓	29.54	92.92
✓	✗	✗	38.67	91.31
✓	✓	✗	27.88	93.28
✓	✗	✓	29.25	93.74
✓	✓	✓	23.65	94.49

Table 3: Ablation study of main components on the ImageNet-1K.

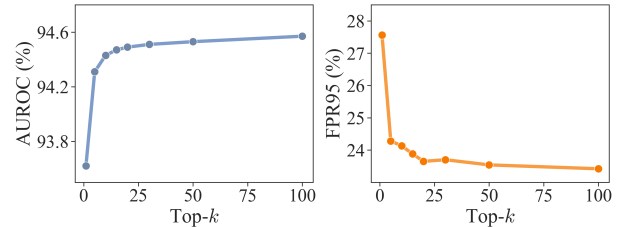


Figure 4: Analyses on the hyper-parameter of threshold k , where results are reported with ImageNet-1K benchmark.

of 43.76%, performing on par with the baseline. This suggests that S_{dist} primarily captures global distributional discrepancy. However, combining S_{dist} with S_{sem} fully leverages their complementary strengths, resulting in a 30.88% improvement in FPR95 and a 2.37% increase in AUROC over the baseline.

Semantic-aware Content Refinement. Comparing the first and fifth rows, as well as the second and fifth rows, shows that SaCR provides moderate improvements when using semantic-based scores. More notably, comparing the third and seventh rows highlights a substantial enhancement in S_{dist} with SaCR, yielding a 33.16% reduction in FPR95 and a 2.99% increase in AUROC. This finding indicates that SaCR introduces distributional shifts that make ID and OOD samples more distinguishable, thereby enabling our OOD score to more effectively capture these differences and enhancing the discriminative power of S_{dist} . Finally, comparing the fourth and last rows shows that applying SaCR to the OT-based OOD score yields a further 19.94% reduction in FPR95 and a 1.66% increase in AUROC. These results confirm the effectiveness of SaCR in our OT-DETECTOR, significantly boosting OOD detection performance.

α	iNaturalist		SUN		Places		Texture	
	FPR95↓	AUROC↑	FPR95↓	AUROC↑	FPR95↓	AUROC↑	FPR95↓	AUROC↑
0	10.45	97.68	18.45	95.94	27.43	93.30	60.67	88.06
0.1	8.65	97.95	16.65	96.11	27.37	93.21	54.40	89.12
0.2	8.10	98.09	16.18	96.15	27.44	92.98	49.27	89.75
0.3	7.91	98.16	16.47	96.11	28.28	92.68	46.81	90.09
0.4	8.05	98.18	17.00	96.01	29.22	92.35	44.73	90.27
0.5	8.22	98.17	17.83	95.89	30.31	92.00	43.95	90.34
0.6	8.53	98.13	18.63	95.74	31.28	91.65	43.07	90.34
0.7	8.84	98.08	19.35	95.57	32.60	91.31	42.85	90.30
0.8	9.25	98.01	20.23	95.38	33.75	90.97	42.77	90.23
0.9	9.79	97.92	21.20	95.19	34.74	90.63	43.05	90.14
1	10.44	97.82	22.07	94.98	35.83	90.30	43.19	90.03

Table 4: Effect of weight α for each score in Eq. (17). The ID dataset is ImageNet-1K. α used for different OOD datasets are highlighted.

4.4 Sensitivity Analysis

Top- k in Eq. 10. Figure 4 shows the effect of varying Top- k (i.e., $k \in \{1, 5, 10, 15, 20, 30, 50, 100\}$) on the performance of our SaCR module. After filtering views for semantic consistency, SaCR selects the top- k views based on their confidence scores for fusion. Since higher-confidence views typically contain more informative content, they are prioritized for feature refinement. As presented in Figure 4, the largest performance gain occurs at $k = 100$. But increasing k introduces additional views of lower confidence, resulting in only marginal changes to the fused features. To balance between capturing sufficiently informative views and avoiding redundancy, we set $k = 20$ by default.

Hyper-parameter α in Eq. 17. Table 4 provides a detailed analysis of α values ranging from 0 to 1 in increments of 0.1. We can see that incorporating both scores with a proper balance consistently yields better performance, as dataset statistics can vary substantially and thus favor different scoring components. For the SUN and Places datasets, the distribution-wise score ($\alpha = 0$) surpasses the semantic-wise score ($\alpha = 1$). In contrast, on the Texture dataset, using only the distribution-wise score performs poorly. Introducing the semantic-wise component ($\alpha > 0$) notably improves FPR95 by 29.01%, suggesting that the large semantic gap between texture images and ImageNet-1K classes benefits significantly from semantic alignment. These observations demonstrate that our score function can adapt effectively to various dataset characteristics by appropriately tuning α .

4.5 Visualization

Case Visualization. Figure 5 illustrates two pairs of ID and hard OOD samples, with ImageNet-100 as the ID dataset and ImageNet-10 as the OOD dataset. Specifically, Figure 5(a) presents the original test images, Figure 5(b) shows the views with the highest confidence selected by SaCR, and Figure 5(c) highlights views with low margins due to insufficient semantic information. For the ID image, SaCR effectively selects views that emphasize the object while eliminating irrelevant background details. In contrast, the hard OOD image in the second column of Figure 5(a) is initially misclassified by CLIP as the “jay” class, and then SaCR selects views focusing on the object parts most resembling the “jay” concept, specifically the bird’s tail, as depicted in the second image of Figure 5(b). As a result, the fused features of the ID and hard OOD samples become significantly more distinct, enhancing their distributional discrepancy. Through this re-

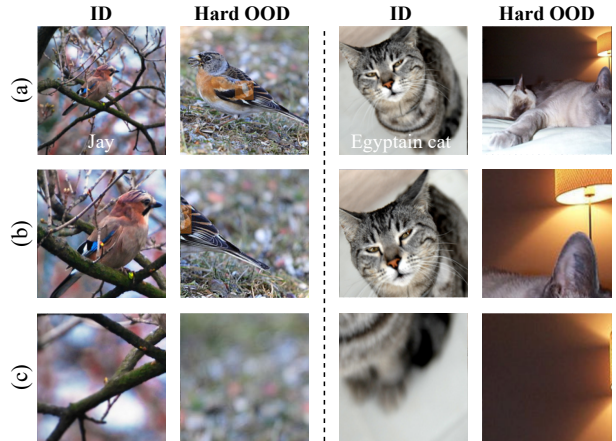


Figure 5: Visualization of SaCR for ID/Hard OOD sample pairs: (a) Test Images; (b) Views selected with largest margin; (c) Views filtered with lower margin.

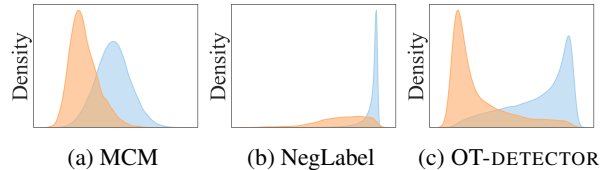


Figure 6: Score distribution of the ID/OOD score with ImageNet-1K/Places as ID/OOD data.

finement, SaCR automatically identifies relevant parts of the hard OOD samples, thereby amplifying the gap between ID and hard OOD samples. This enhanced separation is then captured by the OT-based OOD score function, which leads to improved detection of hard OOD samples.

Score Distribution. Figure 6 presents the density plots of ID and OOD scores for MCM [Ming *et al.*, 2022a], NegLabel [Jiang *et al.*, 2024], and OT-DETECTOR, using the ImageNet-1K dataset as ID data and the Places dataset as OOD data. In Figure 6(a), MCM exhibits a bimodal distribution for both ID and OOD scores. However, a significant overlap exists between the two distributions, making it difficult to determine a suitable threshold for effectively distinguishing OOD data from ID data. Figure 6(b) shows the score distribution for NegLabel. The introduction of numerous negative labels causes ID scores to cluster at higher values due to the negative mining process, which relies on words that are semantically dissimilar to ID labels. However, when OOD images share certain semantic similarity with ID data, the mined negative labels fail to match well, resulting in high confidence scores for many OOD samples. In contrast, Figure 6(c) illustrates the density plot for OT-DETECTOR, revealing a clear bimodal distribution with substantially reduced overlap between ID and OOD scores relative to MCM. This distinct separation of distributions enables more effective threshold selection, thereby leading to superior OOD detection performance by OT-DETECTOR.

5 Conclusion

In this paper, we presented a novel and effective framework for zero-shot OOD detection, termed OT-DETECTOR, by incorporating Optimal Transport to quantify semantic and distributional discrepancies. Building upon this foundation, we devised an OT-based OOD score function that integrates both semantic and distributional scores. Furthermore, to tackle the challenge of hard OOD detection without relying on external knowledge, we introduced a semantic-aware content refinement module, which adaptively amplifies the distinction between ID and hard OOD samples. Extensive experiments demonstrate that OT-DETECTOR achieves state-of-the-art results across various zero-shot detection benchmarks and excels in detecting hard OOD samples.

References

- [Arjovsky *et al.*, 2017] Martín Arjovsky, Soumith Chintala, and Léon Bottou. Wasserstein generative adversarial networks. In *ICML*, volume 70, pages 214–223, 2017.
- [Bossard *et al.*, 2014] Lukas Bossard, Matthieu Guillaumin, and Luc Van Gool. Food-101 - mining discriminative components with random forests. In *ECCV*, volume 8694, pages 446–461, 2014.
- [Cao *et al.*, 2024] Chentao Cao, Zhun Zhong, Zhanke Zhou, Yang Liu, Tongliang Liu, and Bo Han. Envisioning outlier exposure by large language models for out-of-distribution detection. In *ICML*, 2024.
- [Chauhan *et al.*, 2022] Kushal Chauhan, Barath Mohan Umapathi, Pradeep Shenoy, Manish Gupta, and Devarajan Sridharan. Robust outlier detection by de-biasing VAE likelihoods. In *CVPR*, pages 9871–9880, 2022.
- [Cimpoi *et al.*, 2014] Mircea Cimpoi, Subhansu Maji, Iasonas Kokkinos, Sammy Mohamed, and Andrea Vedaldi. Describing textures in the wild. In *CVPR*, pages 3606–3613, 2014.
- [Courty *et al.*, 2017] Nicolas Courty, Rémi Flamary, Devis Tuia, and Alain Rakotomamonjy. Optimal transport for domain adaptation. *IEEE Trans. Pattern Anal. Mach. Intell.*, 39(9):1853–1865, 2017.
- [Cuturi, 2013] Marco Cuturi. Sinkhorn distances: Light-speed computation of optimal transport. In *NIPS*, pages 2292–2300, 2013.
- [Damodaran *et al.*, 2018] Bharath Bhushan Damodaran, Benjamin Kellenberger, Rémi Flamary, Devis Tuia, and Nicolas Courty. Deepjdot: Deep joint distribution optimal transport for unsupervised domain adaptation. In *ECCV (4)*, volume 11208 of *Lecture Notes in Computer Science*, pages 467–483, 2018.
- [Du *et al.*, 2022] Xuefeng Du, Gabriel Gozum, Yifei Ming, and Yixuan Li. SIREN: shaping representations for detecting out-of-distribution objects. In *NeurIPS*, 2022.
- [Esmaeilpour *et al.*, 2022] Sepideh Esmaeilpour, Bing Liu, Eric Robertson, and Lei Shu. Zero-shot out-of-distribution detection based on the pre-trained model CLIP. In *AAAI*, pages 6568–6576, 2022.
- [Fort *et al.*, 2021] Stanislav Fort, Jie Ren, and Balaji Lakshminarayanan. Exploring the limits of out-of-distribution detection. In *NeurIPS*, pages 7068–7081, 2021.
- [Ge *et al.*, 2021] Zheng Ge, Songtao Liu, Zeming Li, Osamu Yoshie, and Jian Sun. OTA: optimal transport assignment for object detection. In *CVPR*, pages 303–312, 2021.
- [Ghosal *et al.*, 2024] Soumya Suvra Ghosal, Yiyu Sun, and Yixuan Li. How to overcome curse-of-dimensionality for out-of-distribution detection? In *AAAI*, pages 19849–19857, 2024.
- [Hendrycks and Gimpel, 2017] Dan Hendrycks and Kevin Gimpel. A baseline for detecting misclassified and out-of-distribution examples in neural networks. In *ICLR*, 2017.
- [Horn *et al.*, 2018] Grant Van Horn, Oisín Mac Aodha, Yang Song, Yin Cui, Chen Sun, Alexander Shepard, Hartwig Adam, Pietro Perona, and Serge J. Belongie. The inaturalist species classification and detection dataset. In *CVPR*, pages 8769–8778, 2018.
- [Huang *et al.*, 2021] Rui Huang, Andrew Geng, and Yixuan Li. On the importance of gradients for detecting distributional shifts in the wild. In *NeurIPS*, pages 677–689, 2021.
- [Jiang *et al.*, 2024] Xue Jiang, Feng Liu, Zhen Fang, Hong Chen, Tongliang Liu, Feng Zheng, and Bo Han. Negative label guided OOD detection with pretrained vision-language models. In *ICLR*, 2024.
- [Kong and Ramanan, 2021] Shu Kong and Deva Ramanan. OpeNgan: Open-set recognition via open data generation. In *ICCV*, pages 793–802. IEEE, 2021.
- [Krause *et al.*, 2013] Jonathan Krause, Michael Stark, Jia Deng, and Li Fei-Fei. 3d object representations for fine-grained categorization. In *ICCV Workshops*, pages 554–561, 2013.
- [Lee *et al.*, 2018] Kimin Lee, Kibok Lee, Honglak Lee, and Jinwoo Shin. A simple unified framework for detecting out-of-distribution samples and adversarial attacks. In *NeurIPS*, pages 7167–7177, 2018.
- [Liang *et al.*, 2018] Shiyu Liang, Yixuan Li, and R. Srikant. Enhancing the reliability of out-of-distribution image detection in neural networks. In *ICLR*, 2018.
- [Liu *et al.*, 2020] Weitang Liu, Xiaoyun Wang, John D. Owens, and Yixuan Li. Energy-based out-of-distribution detection. In *NeurIPS*, 2020.
- [Liu *et al.*, 2023] Zhenzhen Liu, Jin Peng Zhou, Yufan Wang, and Kilian Q. Weinberger. Unsupervised out-of-distribution detection with diffusion inpainting. In *ICML*, volume 202, pages 22528–22538, 2023.
- [Lu *et al.*, 2023] Fan Lu, Kai Zhu, Wei Zhai, Kecheng Zheng, and Yang Cao. Uncertainty-aware optimal transport for semantically coherent out-of-distribution detection. In *CVPR*, pages 3282–3291, 2023.
- [Ming *et al.*, 2022a] Yifei Ming, Ziyang Cai, Jiuxiang Gu, Yiyu Sun, Wei Li, and Yixuan Li. Delving into out-of-distribution detection with vision-language representations. In *NeurIPS*, 2022.

- [Ming *et al.*, 2022b] Yifei Ming, Ying Fan, and Yixuan Li. POEM: out-of-distribution detection with posterior sampling. In *ICML*, volume 162, pages 15650–15665, 2022.
- [Miyai *et al.*, 2023] Atsuyuki Miyai, Qing Yu, Go Irie, and Kiyoharu Aizawa. Zero-shot in-distribution detection in multi-object settings using vision-language foundation models, 2023.
- [Parkhi *et al.*, 2012] Omkar M. Parkhi, Andrea Vedaldi, Andrew Zisserman, and C. V. Jawahar. Cats and dogs. In *CVPR*, pages 3498–3505, 2012.
- [Radford *et al.*, 2021] Alec Radford, Jong Wook Kim, Chris Hallacy, Aditya Ramesh, Gabriel Goh, Sandhini Agarwal, Girish Sastry, Amanda Askell, Pamela Mishkin, Jack Clark, Gretchen Krueger, and Ilya Sutskever. Learning transferable visual models from natural language supervision. In *ICML*, volume 139, pages 8748–8763, 2021.
- [Ren *et al.*, 2019] Jie Ren, Peter J. Liu, Emily Fertig, Jasper Snoek, Ryan Poplin, Mark A. DePristo, Joshua V. Dillon, and Balaji Lakshminarayanan. Likelihood ratios for out-of-distribution detection. In *NeurIPS*, pages 14680–14691, 2019.
- [Ren *et al.*, 2024] Yilong Ren, Chuanwen Feng, Xike Xie, and S. Kevin Zhou. Partial optimal transport based out-of-distribution detection for open-set semi-supervised learning. In *IJCAI*, pages 4851–4859, 2024.
- [Sun *et al.*, 2021] Yiyou Sun, Chuan Guo, and Yixuan Li. React: Out-of-distribution detection with rectified activations. In *NeurIPS*, pages 144–157, 2021.
- [Sun *et al.*, 2022] Yiyou Sun, Yifei Ming, Xiaojin Zhu, and Yixuan Li. Out-of-distribution detection with deep nearest neighbors. In *ICML*, volume 162, pages 20827–20840, 2022.
- [Tack *et al.*, 2020] Jihoon Tack, Sangwoo Mo, Jongheon Jeong, and Jinwoo Shin. CSI: novelty detection via contrastive learning on distributionally shifted instances. In *NeurIPS*, 2020.
- [Wah *et al.*, 2011] C. Wah, S. Branson, P. Welinder, P. Perona, and S. Belongie. Technical Report CNS-TR-2011-001, California Institute of Technology, 2011.
- [Wang *et al.*, 2022] Haoqi Wang, Zhizhong Li, Litong Feng, and Wayne Zhang. Vim: Out-of-distribution with virtual-logit matching. In *CVPR*, pages 4911–4920, 2022.
- [Wang *et al.*, 2023] Hualiang Wang, Yi Li, Huifeng Yao, and Xiaomeng Li. CLIPN for zero-shot OOD detection: Teaching CLIP to say no. In *ICCV*, pages 1802–1812, 2023.
- [Xiao *et al.*, 2010] Jianxiong Xiao, James Hays, Krista A. Ehinger, Aude Oliva, and Antonio Torralba. SUN database: Large-scale scene recognition from abbey to zoo. In *CVPR*, pages 3485–3492, 2010.
- [Xiao *et al.*, 2020] Zhisheng Xiao, Qing Yan, and Yali Amit. Likelihood regret: An out-of-distribution detection score for variational auto-encoder. In *NeurIPS*, 2020.
- [Yang *et al.*, 2021] Jingkang Yang, Haoqi Wang, Litong Feng, Xiaopeng Yan, Huabin Zheng, Wayne Zhang, and Ziwei Liu. Semantically coherent out-of-distribution detection. In *ICCV*, pages 8281–8289, 2021.
- [Yang *et al.*, 2023] Yucheng Yang, Xiang Gu, and Jian Sun. Prototypical partial optimal transport for universal domain adaptation. In *AAAI*, pages 10852–10860, 2023.
- [Yang *et al.*, 2024] Jingkang Yang, Kaiyang Zhou, Yixuan Li, and Ziwei Liu. Generalized out-of-distribution detection: A survey. *Int. J. Comput. Vis.*, 132(12):5635–5662, 2024.
- [Zhou *et al.*, 2018] Bolei Zhou, Àgata Lapedriza, Aditya Khosla, Aude Oliva, and Antonio Torralba. Places: A 10 million image database for scene recognition. *IEEE Trans. Pattern Anal. Mach. Intell.*, 40(6):1452–1464, 2018.

A Appendix

This appendix provides supplementary materials and detailed discussions to support the main content of the paper. Specifically:

- **Section A.1** offers a comprehensive review of related works.
- **Section A.2** presents extensive evaluations of our OT-DETECTOR using various prompt templates.
- **Section A.3** reports experimental results of our OT-DETECTOR on additional tasks.
- **Sections A.4 and A.5** contain further experimental results on the components of our OT-DETECTOR.
- **Section A.6** validates the effectiveness of our OT-DETECTOR using different versions of CLIP.
- **Section A.7** discusses the limitations of our OT-DETECTOR and proposes potential future directions.
- **Section A.8** provides a comparative analysis of the strengths and weaknesses of NegLabel in relation to our OT-DETECTOR.

A.1 Related Works

OOD Detection. OOD detection aims to identify inputs that deviate semantically from the training data. This task is typically categorized into three main approaches: score-based methods [Yang *et al.*, 2021; Ming *et al.*, 2022b; Wang *et al.*, 2022], distance-based approaches [Tack *et al.*, 2020; Sun *et al.*, 2022; Du *et al.*, 2022; Ghosal *et al.*, 2024], and generative-based approaches [Xiao *et al.*, 2020; Ren *et al.*, 2019; Kong and Ramanan, 2021; Chauhan *et al.*, 2022]. Score-based methods typically design a score function based on the model’s uncertainty for a given test input, which is then used to determine whether the input is OOD. For instance, [Hendrycks and Gimpel, 2017] introduce the maximum softmax probability as a baseline for OOD detection. Additionally, [Liang *et al.*, 2018] observe that adversarial perturbations during training can improve OOD detection, while [Liu *et al.*, 2020] propose the energy score, which aligns with the probability density for OOD detection. ReAct [Sun *et al.*, 2021] improves OOD detection by dynamically adjusting confidence thresholds and incorporating rejection regions. Mahalanobis distance-based method [Lee *et al.*, 2018] leverages class-conditional feature distributions to measure the likelihood of a sample being OOD. More recently, [Liu *et al.*, 2023] utilize the manifold mapping capability of diffusion models, employing a standard image similarity metric to quantify the distance between original and reconstructed images for OOD detection. However, these methods often rely solely on the visual modality and exhibit suboptimal performance when applied to large-scale benchmarks. To address this, recent advances in zero-shot OOD detection that integrate Vision-Language Models (VLM) with OOD detection have shown promising results.

Zero-shot OOD Detection. Zero-shot OOD detection aims to identify samples that do not belong to any ID class described by user-provided text, leveraging the semantic understanding capabilities of vision-language models (VLMs).

Most existing methods identify OOD samples based on the cosine similarity between visual and textual features. For example, MCM [Ming *et al.*, 2022a] uses the maximum temperature-scaled softmax value between the textual features of ID labels and the visual features of test images as the OOD score. Building on MCM, GL-MCM [Miyai *et al.*, 2023] incorporates background information, designing a global OOD score that also accounts for the similarity between background features and textual features. ZOC [Esmaeilpour *et al.*, 2022] introduces an additional text decoder as a captioner to generate candidate OOD labels for test data. Similarly, CLIPN [Wang *et al.*, 2023] trains an additional text encoder to enable CLIP to effectively handle negative prompts. EOE [Cao *et al.*, 2024] leverages large language models (LLMs) by designing prompts to guide LLMs in generating candidate OOD labels, improving OOD detection performance. However, the labels generated through LLMs lack sufficient diversity, which consequently reduces the performance of OOD detection. NegLabel [Jiang *et al.*, 2024] introduces a NegMining algorithm to extract candidate OOD labels by selecting semantically distant words from WordNet. It designs an OOD score based on the similarity to these negative labels. However, since OOD samples may exhibit a certain degree of semantic similarity to ID samples, these negative labels often struggle to align with such OOD samples, leading to limited OOD detection performance.

Optimal Transport. Optimal Transport (OT), a mathematical tool for measuring distributional discrepancies, has been widely adopted in various fields. In domain adaptation [Courty *et al.*, 2017; Yang *et al.*, 2023; Damodaran *et al.*, 2018], OT is used to align source and target domains. Wasserstein GAN [Arjovsky *et al.*, 2017] leverages OT to measure distributional distance, using it as a loss function for training the generator. In object detection, [Ge *et al.*, 2021] applies OT to address the matching problem between anchors and ground truth. Several works explore OT in Out-of-Distribution (OOD) detection [Ren *et al.*, 2024; Lu *et al.*, 2023]. [Ren *et al.*, 2024] introduces Partial OT to Open-Set Semi-Supervised Learning (OSSSL), reallocating weights for unlabeled samples to align their distribution with the labeled data, enhancing interpretability in OOD detection. Similarly, [Lu *et al.*, 2023] combines OT with clustering methods, leveraging distributional discrepancies between ID and OOD samples to assign unlabeled samples to appropriate clusters.

To the best of our knowledge, the application of OT in the zero-shot OOD detection realm remains unexplored. Existing methods use OT to model relationships between labeled training data (i.e., ID samples) and unlabeled data. In this work, we propose a zero-shot OOD detection framework that integrates OT with an OOD score, incorporating both semantic and distributional scores for improved detection performance.

A.2 Effect of Prompt Engineering

We evaluate the impact of various prompt templates on the ImageNet-1K benchmark, as summarized in Table 5. Our method demonstrates consistent performance across a wide range of prompt templates, highlighting its robustness to

Prompt Templates	OOD Dataset									
	iNaturalist		SUN		Places		Texture		Average	
	FPR95↓	AUROC↑	FPR95↓	AUROC↑	FPR95↓	AUROC↑	FPR95↓	AUROC↑	FPR95↓	AUROC↑
A bad photo of the [CLASS].	11.87	97.48	19.63	95.47	32.24	92.02	42.62	91.20	26.59	94.05
A tattoo of a [CLASS].	6.35	98.46	14.63	96.72	26.88	93.43	47.62	88.48	23.87	94.27
A bright photo of a [CLASS].	8.75	97.89	16.29	96.17	29.01	92.84	43.23	90.25	24.32	94.29
A photo of a clean [CLASS].	8.22	98.04	17.53	95.91	28.34	92.97	42.39	90.19	24.12	94.28
A photo of a dirty [CLASS].	9.38	97.82	16.86	96.00	31.06	92.16	44.80	89.23	25.53	93.80
A low resolution photo of a [CLASS].	9.53	97.82	20.80	95.12	30.77	92.41	42.64	90.12	25.94	93.87
A photo of a cool [CLASS].	7.85	98.18	15.26	96.42	28.61	92.72	43.99	90.18	23.93	94.38
A photo of a small [CLASS].	8.49	97.86	17.41	95.91	27.05	93.38	41.95	90.80	23.73	94.49
A dark photo of a [CLASS].	8.63	98.02	17.86	96.05	30.97	92.12	44.41	89.41	25.47	93.90
A blurry photo of a [CLASS].	10.70	97.63	20.07	95.03	31.53	91.19	42.16	90.30	26.12	93.54
A low resolution photo of a [CLASS].	9.53	97.82	20.80	95.12	30.77	92.41	42.64	90.12	25.94	93.87
A cropped photo of the [CLASS].	9.99	97.70	20.36	95.37	29.86	92.63	43.16	90.19	25.84	93.97
A good photo of a [CLASS].	7.87	98.13	14.53	96.51	29.06	92.59	43.01	90.66	23.62	94.47
[CLASS].	8.91	98.03	15.83	96.38	24.26	93.82	42.29	90.96	22.82	94.80
A photo of a [CLASS].	7.91	98.16	16.18	96.15	27.43	93.30	43.07	90.34	23.65	94.49
The nice [CLASS].	7.85	98.19	16.72	96.22	25.63	93.44	35.73	92.70	21.48	95.14
The nice cropped [CLASS].	11.41	97.43	20.41	95.57	29.40	92.76	41.49	91.61	25.68	94.34
The nice complete [CLASS].	6.63	98.44	16.50	96.38	23.18	94.13	39.18	91.86	21.37	95.20

Table 5: Performance comparison with different prompts on the ImageNet-1K benchmark.

ID Dataset	Method	OOD Dataset									
		iNaturalist		SUN		Places		Texture		Average	
		FPR95↓	AUROC↑	FPR95↓	AUROC↑	FPR95↓	AUROC↑	FPR95↓	AUROC↑	FPR95↓	AUROC↑
CUB-200	MCM	9.83	98.24	4.93	99.10	6.65	98.57	6.97	98.75	7.09	98.66
	OT-DETECTOR	6.73	98.64	0.02	99.99	0.52	99.85	0.02	99.99	0.17	99.95
Stanford-Cars	MCM	0.05	99.77	0.02	99.95	0.24	99.89	0.02	99.96	0.08	99.89
	OT-DETECTOR	0.00	100.00	0.00	100.00	0.09	99.97	0.00	100.00	0.02	99.99
Food-101	MCM	0.64	99.78	0.90	99.75	1.86	99.58	4.04	98.62	1.86	99.43
	OT-DETECTOR	0.22	99.96	0.13	99.97	0.47	99.92	5.05	98.32	1.47	99.54
Oxford-Pet	MCM	2.85	99.38	1.06	99.73	2.11	99.56	0.80	99.81	1.70	99.62
	OT-DETECTOR	0.00	99.99	0.03	99.99	0.19	99.95	0.20	99.95	0.10	99.69
ImageNet-10	MCM	0.12	99.80	0.29	99.79	0.88	99.62	0.04	99.90	0.33	99.78
	OT-DETECTOR	0.08	99.82	0.22	99.74	0.72	99.56	0.07	99.84	0.27	99.74
ImageNet-20	MCM	1.02	99.66	2.55	99.50	4.40	99.11	2.43	99.03	2.60	99.32
	OT-DETECTOR	0.73	99.80	2.69	99.45	3.66	99.25	2.25	98.98	2.34	99.37
ImageNet-100	MCM	18.13	96.77	36.45	94.54	34.52	94.36	41.22	92.25	32.58	94.48
	OT-DETECTOR	4.87	98.99	8.83	97.86	17.27	96.53	24.40	95.78	13.84	97.29

Table 6: Zero-shot OOD detection performance comparison on various ID datasets.

prompt variations. Notably, the template “the nice [CLASS].” achieves the best performance.

To further investigate, we modify the template by adding “cropped” and “complete”, resulting in “the nice cropped [CLASS].” and “the nice complete [CLASS].” templates. As shown in the last three rows of Table 5, using “the nice cropped [CLASS].” leads to a significant performance drop, whereas “the nice complete [CLASS].” improves performance further. We attribute these results to the Semantic-aware Content Refinement (SaCR) module. SaCR retains the full object in ID images, while OOD images often contain only partial objects. Using “cropped” in the template increases the similarity between textual features and OOD images, causing a noticeable degradation in performance. Conversely, “complete” emphasizes the full object, enhancing the separation between ID and OOD samples and improving detection performance.

A.3 Evaluation on Various ID Datasets

To further validate the efficacy of our method, we perform experiments on additional datasets. Following the setup in

MCM [Ming *et al.*, 2022a], we use subsets of ImageNet, CUB-200 [Wah *et al.*, 2011], Stanford Cars [Krause *et al.*, 2013], Food-101 [Bossard *et al.*, 2014], and Oxford Pets [Parkhi *et al.*, 2012] as ID data, while utilizing iNaturalist, SUN, Places, and Textures as OOD data. The results, summarized in Table 6, demonstrate that our method achieves an FPR95 of approximately 1% and an AUROC near 100% on CUB-200, Stanford Cars, Food-101, Oxford Pets, ImageNet-10, and ImageNet-20. On the ImageNet-100 dataset, our approach improves FPR95 by 57.52% and AUROC by 2.89%, yielding substantial performance improvements. These findings underscore the robustness and generalizability of our method across various datasets.

A.4 More Experiments on Optimal Transport

This section investigates the impact of the hyperparameter ϵ in the entropy regularization term and the cost matrix C in Eq. 14.

Sensitivity Analysis on Hyperparameter ϵ . The regularization parameter ϵ plays a crucial role in balancing the trade-off between smoothness and computational complexity, influ-

ϵ	OOD Dataset									
	iNaturalist		SUN		Places		Texture		Average	
	FPR95↓	AUROC↑	FPR95↓	AUROC↑	FPR95↓	AUROC↑	FPR95↓	AUROC↑	FPR95↓	AUROC↑
50	16.21	96.78	30.50	93.75	40.03	90.86	46.06	89.32	33.20	92.68
60	11.55	97.49	24.52	94.79	35.56	91.94	44.88	89.78	29.13	93.50
70	9.33	97.87	19.90	95.52	31.02	92.68	43.99	90.12	26.06	94.05
80	8.26	98.09	17.41	95.94	29.23	93.10	43.40	90.33	24.58	94.36
90	7.91	98.16	16.18	96.15	27.43	93.30	43.07	90.34	23.65	94.49
100	7.92	98.15	15.58	96.22	27.05	93.36	43.21	90.21	23.44	94.49
110	8.08	98.14	15.52	96.22	26.75	93.35	43.78	89.97	23.53	94.42
120	8.45	98.10	15.57	96.17	26.74	93.29	43.87	89.71	23.66	94.32
130	8.97	97.98	15.83	96.11	27.05	93.22	44.33	89.41	24.04	94.18
140	9.34	97.91	16.11	96.03	27.39	93.14	44.91	89.11	24.44	94.05
150	9.75	97.83	16.34	95.94	27.75	93.05	45.55	88.81	24.85	93.91

Table 7: Detailed results on the impact of different ϵ with ImageNet-1k benchmark.

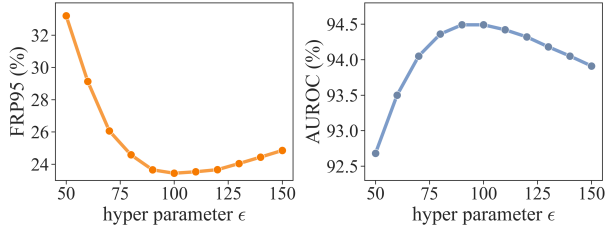


Figure 7: Analyses on the regularization parameter ϵ , where results are reported with ImageNet-1k benchmark.

encing the "softness" of the optimal transport solution [Cuturi, 2013]. As shown in Figure 7, the optimal value of ϵ for FPR95 is around 100, where the minimum value is achieved. For AUROC, the maximum is attained at approximately 90. Based on these observations, we select $\epsilon = 90$ for all subsequent experiments. Table 7 further presents the effect of varying ϵ on four OOD datasets from the ImageNet-1K benchmark. The results indicate that the optimal ϵ varies slightly across different datasets, with $\epsilon = 90$ yielding satisfactory performance on all four datasets.

Choice of Cost Matrix C . We perform a comparative evaluation of cosine distance and L2 distance as the cost matrix on the ImageNet-1K benchmark, as summarized in Table 8. The results show a significant performance improvement with cosine distance, suggesting that it is a more suitable measure for the distance between CLIP’s textual and visual features.

Metric	FPR95↓	AUROC↑
L2 distance	25.57	94.15
Cosine distance	23.65	94.49

Table 8: Different cost metrics evaluated with the ImageNet-1K benchmark.

A.5 Additional Experiments on the SaCR Module

This section discusses the number of views N in **view augmentation**, the selection of the confidence function, and the constraint on maintaining consistency in view labels during **view selection**.

SaCR	Label Consistency	FPR95↓	AUROC↑
✗	✗	32.65	94.96
✓	✗	24.42	95.82
✓	✓	22.60	96.15

Table 9: Effect of the Semantic Guidance with ImageNet-100/ImageNet-10 as ID/OOD data.

Sensitive Analysis of the View Number N . We conduct experiments on the ImageNet-1K benchmark to evaluate the impact of the number of views N on zero-shot OOD detection performance, as shown in Table 10. Here, $N = 1$ denotes the use of only the original image. The augmentation step primarily affects the degree of decoupling of the original image content. Increasing N generally enhances the ability to capture more diverse object parts that convey semantic information from the original image, thus influencing the quality of the refined features obtained through fusion. Table 10 demonstrates that using only the original image ($N = 1$) yields the lowest performance. As N increases, performance steadily improves, indicating that additional views facilitate the extraction of more local features, which helps to capture more comprehensive and semantically relevant regions in OOD samples that correspond to the ID samples.

Choice of Confidence Function. We investigate the impact of various confidence functions on view selection, as shown in Table 11. The primary confidence functions considered include *min-entropy*, *min-margin*, and *max-margin*. Specifically, the min-entropy method computes the self-entropy for each view and selects the view with the lowest entropy value, yielding satisfactory performance. Among the evaluated strategies, the max-margin approach demonstrates the best performance.

Impact of Maintaining View Label Consistency. We conduct ablation experiments using ImageNet-100/ImageNet-10 as the ID/OOD data to validate the effectiveness of maintaining label consistency in view selection within SaCR. The experimental results, presented in Table 9, show that view selection based on confidence scores leads to significant performance improvements even without label consistency. Incorporating label consistency into SaCR further enhances the results, achieving a notable reduction in FPR95 by 30.78%. This demonstrates the effectiveness of SaCR in addressing

N Views	OOD Dataset									
	iNaturalist		SUN		Places		Texture		Average	
	FPR95↓	AUROC↑	FPR95↓	AUROC↑	FPR95↓	AUROC↑	FPR95↓	AUROC↑	FPR95↓	AUROC↑
1	10.44	97.69	22.72	95.07	35.16	91.66	49.84	87.25	29.54	92.92
8	10.65	97.61	23.31	94.94	34.05	92.07	46.63	89.16	28.66	93.45
32	9.21	97.91	20.08	95.50	31.39	92.70	44.11	89.97	26.20	94.02
64	8.18	98.11	18.04	95.91	29.80	93.14	44.72	89.97	25.18	94.28
128	8.20	98.11	17.61	95.92	29.23	93.13	44.31	90.15	24.84	94.33
256	7.91	98.16	16.18	96.15	27.43	93.30	43.07	90.34	23.65	94.49

Table 10: Effect of the views number N , where experiments are conducted with ImageNet-1K benchmark.

Confidence Function	FPR95↓	AUROC↑
Min-Entropy	24.16	94.35
Min-Margin	28.51	93.39
Max-Margin	23.65	94.49

Table 11: Performance comparison of different confidence functions, evaluated with the ImageNet-1K benchmark.

the challenging problem of hard OOD detection. To further illustrate the impact of SaCR, we compare the density plots of ID and OOD scores before and after applying SaCR, as shown in Figure 8. The results indicate that SaCR reduces sensitivity to threshold selection when distinguishing between ID and OOD samples. Additionally, ID scores are significantly elevated, highlighting a clearer separation between ID and OOD distributions.

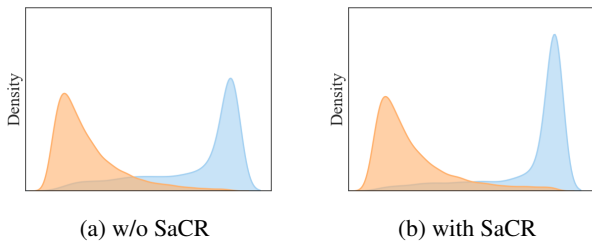


Figure 8: Score distribution of the ID (blue) and OOD (orange) score w/o SaCR (left) and with SaCR (right).

A.6 Evaluation with Different Versions of CLIP

In this section, we evaluate the performance of OT-DETECTOR using different CLIP versions and compare it with two competitive methods, EOE and NegLabel. Table 12 presents the results on the ImageNet-1K benchmark for various CLIP versions, including ViT-B/32, ViT-B/16, and ResNet50. Our method achieves the best performance across both convolutional and attention-based vision encoders, demonstrating the strong generalization capability of our approach across different visual architectures.

A.7 Limitation

Sensitivity to Different Batch Sizes. Due to the inherent limitations of Optimal Transport (OT), OT-DETECTOR requires a sufficient number of test features to quantify the distributional discrepancy between the test features and the ID

textual features using OT, and subsequently identify OOD samples based on the OOD score S_{OT} . It is important to note that our method does not rely on the labels of the test data. Instead, it only requires the cosine distance between batches of test data features and the ID label features. OT optimization is then performed based on these cosine distances. Therefore, unlike methods such as MCM and NegLabel, our approach cannot provide real-time evaluations for individual test samples.

The use of OT also introduces sensitivity to batch size, as larger batches allow the observed distribution to better approximate the true distribution of the test data. To evaluate this, we conduct experiments with varying batch sizes using the ImageNet-1K benchmark, as shown in Table 13. The results show that as the batch size increases, the performance of our method improves, reaching its peak when the entire test dataset is utilized.

In future work, we aim to further explore the integration of OT with zero-shot OOD detection to improve performance with smaller batch sizes, thereby enhancing the practicality and efficiency of the approach in real-world applications.

Requirement for Sufficient ID Labels. As shown in Table 2, OT-DETECTOR achieves an FPR95 of 3.06% and an AUROC of 99.17% when using ImageNet-10 as ID data and ImageNet-100 as OOD data. While this performance is slightly lower than that of MCM, it still represents a commendable result. We attribute this to the fact that when ImageNet-10 is used as ID data, the number of ID labels is significantly smaller than the number of categories in the OOD data. In such an imbalanced scenario, the semantic information provided by the ID labels is insufficient to generate sufficiently effective views of the OOD data with complex categories, thereby limiting the effectiveness of SaCR. However, when a sufficient number of ID categories is available, such as when using ImageNet-100/ImageNet-10 as ID/OOD data, our method outperforms others, even significantly surpassing NegLabel.

A.8 Discussion on NegLabel

As shown in Table 1, when compared to NegLabel [Jiang *et al.*, 2024], our approach exhibits slightly inferior performance on the iNaturalist dataset. However, it shows substantial improvements over NegLabel on the SUN and Places datasets, resulting in superior overall performance. It is important to note that for the ImageNet-1K benchmark, NegLabel utilizes ten times the number of ID labels as negative labels.

Method (CLIP version)	iNaturalist		SUN		OOD Dataset Places		Texture		Average	
	FPR95↓	AUROC↑	FPR95↓	AUROC↑	FPR95↓	AUROC↑	FPR95↓	AUROC↑	FPR95↓	AUROC↑
	EOE (ResNet50)	14.44	97.05	24.85	94.82	38.89	90.64	59.73	85.44	34.47
NegLabel (ResNet50)	2.88	99.24	26.51	94.54	42.60	89.72	50.80	88.40	30.70	92.97
OT-DETECTOR (ResNet50)	12.45	97.19	21.21	95.09	34.87	91.28	49.86	88.43	29.60	93.00
EOE (ViT-B/32)	14.97	97.03	21.88	95.40	29.91	92.97	60.10	84.61	31.72	92.50
NegLabel (ViT-B/32)	3.73	99.11	22.48	95.27	34.94	91.72	50.51	88.57	27.92	93.67
OT-DETECTOR (ViT-B/32)	10.16	97.76	19.26	95.53	27.80	93.20	44.89	89.59	25.53	94.02
EOE (ViT-B/16)	12.29	97.52	20.40	95.73	30.16	92.95	57.53	85.64	30.09	92.96
NegLabel (ViT-B/16)	1.91	99.49	20.53	95.49	35.59	91.64	43.56	90.22	25.40	94.21
OT-DETECTOR (ViT-B/16)	7.91	98.16	16.18	96.15	27.43	93.30	43.07	90.34	23.65	94.49

Table 12: Additional experimental results using different versions of CLIP on the ImageNet-1K benchmark.

Batch	iNaturalist		SUN		OOD Dataset Places		Texture		Average	
	FPR95↓	AUROC↑	FPR95↓	AUROC↑	FPR95↓	AUROC↑	FPR95↓	AUROC↑	FPR95↓	AUROC↑
	16	51.97	89.85	62.12	86.72	63.48	84.81	63.85	84.87	60.35
64	32.00	93.37	47.08	90.44	52.08	88.18	53.69	86.49	46.21	89.62
128	26.58	94.51	43.48	91.22	49.38	88.87	51.60	86.73	42.76	90.33
256	23.12	95.26	38.82	92.20	46.21	89.67	50.16	87.06	39.58	91.05
512	18.89	95.89	35.19	93.07	42.04	90.65	48.78	87.69	36.22	91.82
1024	15.46	96.61	29.22	93.82	38.43	91.24	47.59	88.15	32.67	92.45
2048	12.46	97.24	22.82	94.82	34.09	92.06	46.49	88.66	28.96	93.19
5096	9.51	97.80	19.07	95.55	30.85	92.71	45.71	89.13	26.28	93.79
ALL	7.91	98.16	16.18	96.15	27.43	93.30	43.07	90.34	23.65	94.49

Table 13: Effect of different batch sizes with ImageNet-1K benchmark.

The superior performance of NegLabel on the iNaturalist dataset can be primarily attributed to the nature of iNaturalist, which consists mostly of images of natural plants. In contrast, ImageNet-1K covers a much broader range of categories, predominantly focusing on food and animals. Therefore, iNaturalist differs significantly from ImageNet-1K in terms of category composition. As a result, the negative labels introduced by NegLabel are particularly effective in describing the iNaturalist dataset, even enabling the identification of the ground-truth label for a given image. On the other hand, datasets such as SUN and Places exhibit greater semantic similarity to ImageNet-1K, leading to less effective performance for NegLabel. While our method incorporates additional distributional discrepancy, it is challenging to outperform NegLabel on the iNaturalist dataset. Nevertheless, for the other three OOD datasets, our method demonstrates better performance.

Additionally, as reported in NegLabel, its performance is highly sensitive to the prompt template. Arbitrary modifications to the prompt template can lead to a significant performance drop. Through prompt engineering, NegLabel identifies the template "the nice [CLASS]" as yielding the best results. In contrast, as discussed in Section A.2, OT-DETECTOR consistently delivers stable performance across various templates, demonstrating its strong robustness to variations in the prompt template.